The Elastic Wave Velocity Response of Methane Gas Hydrate Formation in Vertical Gas Migration Systems

Q T Bu[1,2], G W Hu[2,3†], Y G Ye[2,3], C L Liu[2,3], C F Li[2,3], A I Best[4], J S Wang[1†]

[1]State Key Laboratory of Biogeology and Environmental Geology, School of Earth Sciences, China University of Geosciences, Wuhan 430074, China

[2]The Key Laboratory of Gas Hydrate, Ministry of Land and Resources, Qingdao Institute of Marine Geology, Qingdao 266071, China

[3]Laboratory for Marine Mineral Resources, Qingdao National Laboratory for Marine Science and Technology, Qingdao 266071, China

[4]National Oceanography Centre, University of Southampton Waterfront Campus, European Way, Southampton SO14 3ZH, United Kingdom

† Corresponding author: Gaowei Hu, Email: hgw-623@163.com , Current address: 62 Fuzhou South Road Qingdao, China

Jiasheng Wang, Email: js-wang@cug.edu.cn , Current address: No. 388 Lumo Road, Wuhan, China

Abstract

Knowledge of the elastic wave velocities of hydrate-bearing sediments is important for geophysical exploration and resource evaluation. Methane gas migration processes play an important role in geological hydrate accumulation systems, whether on the seafloor or in terrestrial permafrost regions, and their impact on elastic wave velocities in sediments needs further study. Hence, a high pressure laboratory apparatus was developed to simulate natural continuous vertical methane gas migration through sediments. Hydrate saturation (S_h) and ultrasonic P- and S-wave velocities (V_p & V_s) were measured synchronously by time domain reflectometry (TDR) and by ultrasonic transmission methods respectively during gas hydrate formation in sediment. The results were compared to previously published laboratory data obtained in a static closed system. This indicated that the velocities of hydrate-bearing sediments in vertical gas migration systems are slightly lower than

those in closed systems during hydrate formation. While velocities increase at a constant rate with hydrate saturation in the closed system, P-wave velocities show a fast-slow-fast variation with increasing hydrate saturation in the vertical gas migration system. The observed velocities are well described by an effective medium velocity model, from which changing hydrate morphology was inferred to cause the fast-slow-fast velocity response in the gas migration system. Hydrate forms firstly at the grain contacts as cement, then grows within the pore space (floating), then finally grows into contact with the pore walls again. We conclude that hydrate morphology is the key factor that influences the elastic wave velocity response of methane gas hydrates formation in vertical gas migration systems.

Keywords: Gas hydrates; Vertical gas migration system; Elastic wave velocity; Hydrate saturation; Hydrate morphology

1. Introduction

Very large volumes of methane could be present in hydrate accumulations on the deep seafloor and in permafrost regions according to Milkov and Sassen (2003). As such, gas hydrates have been identified as a very important potential energy resource in the 21st century (Collett, 2014; Chong *et al.*, 2015). Geophysical exploration techniques are widely used for natural gas hydrate exploration and resource evaluation (Shipley *et al.*, 1979; Holbrook *et al.*, 1996, 2002; Careione and Gei, 2004) because gas hydrates show higher P and S wave velocities than the sediment/rock pore fluid, typically brine (Stoll, 1974; Tueholke, 1977; Holbrook *et al.*, 1996; Michael, 2003; Waite *et al.*, 2009; Pecher *et al.*, 2010). Since gas hydrates are unstable at room temperatures and pressures, it is rare for both hydrate saturation (S_h) and elastic wave velocities of hydrate-bearing sediments to be measured on core samples recovered in the field, without specialist pressurized coring technologies. To quantify the gas hydrate saturation, and to infer other physical properties of gas hydrate–bearing sediments, a study on the relationship between the gas hydrate saturation and the elastic wave velocities is essential. Simulating natural gas hydrate formation processes in sediments in the laboratory is an effective approach to study elastic wave velocity variations during hydrate formation (e.g. Winters *et al.*, 2007), and can also be used to

verify rock physics models (e.g. Hu *et al.*, 2010c) needed to interpret field seismic data.

To date, experimental studies have been conducted on the elastic wave characteristics of methane hydrate reservoirs under static conditions mostly. Winters *et al.* (2007) studied how gas hydrate influence ultrasonic velocities of different types of sediments, which contains natural samples, synthesized frozen samples and hydrate-bearing sediments. Priest *et al.* (2005, 2009) studied methane hydrate effects on seismic velocity under static "excess gas", "excess water" and "dissolved gas" conditions. Hu *et al.* (2008, 2010b, 2012, 2014a) used ultrasonic method and Time Domain Reflectometry (TDR) techniques to measure real-time hydrate saturation and both V_p and V_s in rocks and sediments, including sediment samples from the South China Sea. These studies led to two important findings: (1) gas hydrate morphology has a significant impact on the elastic wave velocities of hydrate reservoirs; for example, the elastic wave velocity change is most obvious when hydrate cements sand grains; (2) hydrate morphology varies according to the nature of the gas supply; for example, hydrates formed from free gas usually cement sediments, while hydrates formed from dissolved gas tend to float, suspended in the pore fluid (Winters *et al.*, 2007). Biogenic methane production in the hydrate stability zone is generally not sufficient to form the observed amounts of hydrate in hydrate reservoirs, so deep methane supplies below the hydrate stability zone are inferred. Gas migration is likely to be a very significant component of gas hydrate systems (Collett, 2014) and is worthy of detailed study in the laboratory.

Laboratory experimental techniques suitable for simulating vertical gas migration system present the following technical challenges: (1) the gas flow needs to be controlled in order to simulate the natural environment; (2) water in the sediment pore space is easily removed by gas flow; (3) the gas migration channels can become blocked by hydrate formation. In addition, as the acoustic attenuation is significantly large in gas bubble system, it's a challenge to obtain both P- and S- wave characteristics in this system.

Although some researchers have simulated hydrate formation in a dynamic

system, only a few experiments have focused on elastic wave properties, and hydrate saturation was not measured directly during the hydrate formation process. Kwon *et al*. (2009) conducted CO_2 hydrate formation experiments with injecting gas and water mixture from the bottom of the apparatus; the results show that the P- wave velocity increase from 1656 m/s to 1737 m/s at the start of hydrate formation, and the P- wave velocity finally reach 2725 m/s. However, as there is no measured hydrate saturation (S_h), S_h was just estimated by comparing the observations to several rock physics velocity models. Liu *et al*. (2013) used a vertical migration mode for gas supply during CH_4-CO_2 displacement reaction; the results showed that P wave velocity decreased continually during the replacement of CH_4 with CO_2; but no hydrate saturation data was measured. Su *et al*. (2012) developed a seeping system using a large scale simulation device to consider three kinds of gas supply modes for hydrate formation. The hydrate saturation was calculated from the electrical resistivity measurements. Although there was acoustic detection designed in the experiment, there was no acoustic data reported. Similarly, Wang *et al.* (2007) and Guan *et al.* (2012) also developed a leakage system simulator to form hydrate under subsea vertical gas migration conditions, but with no acoustic measurements to date. Eaton *et al.* (2007) developed the FISH (Flexible Integrated Study of Hydrates) experimental apparatus to simulate the real marine environment; water was injected from the top of the sample and gas was injected from below. Acoustic velocities were obtained after hydrate had formed, but no acoustic data were collected during hydrate formation.

In this study, we designed a special high pressure apparatus to study the response of elastic wave velocities and hydrate saturation to gas hydrate formation under vertical gas migration conditions. Several novel aspects were incorporated into an existing experimental system: the pressure control system, the microporous sintered plate, the waterproof sand and the heating plate are applied in the system to ensure gas migrates vertically, and during which hydrate can form smoothly. During the experimental process, the combination of ultrasonic technique and TDR was used to obtain real time ultrasonic wave data and gas hydrate saturation simultaneously. The experimental data was subsequently used to establish the relationship between the

4

velocities and hydrate saturation under vertical gas migration, and present helpful information for interpreting elastic wave phenomenon in gas migrating reservoirs.

2. Experimental Equipment and Materials

The experimental system consists of four units: a high pressure cell, a temperature control system, a pressure control system for gas supply and a computer control system (Figure 1). Two microporous sintered plates were used to divide the high pressure cell space into three parts: an upper gas cell, a lower gas cell, and a space used to hold sediments (where hydrate was formed). The thickness of cell wall is 12 mm and the sealing cap is 38 mm, the inner diameter of the cell is 200 mm. The gas supply system consists of a CH_4 cylinder, a high pressure gas pipeline, a pressure transducer (precision, ± 0.1 MPa) and a gas compressor. Pressure in the cell is measured by a pressure sensor mounted on the gas supply line, and the measuring range is 0~35 MPa with precision of ± 0.1 MPa. The cell is placed in a cold air bath to control its temperature. The temperature range is -30 ℃~ room temperature (precision, ± 0.5 ℃).
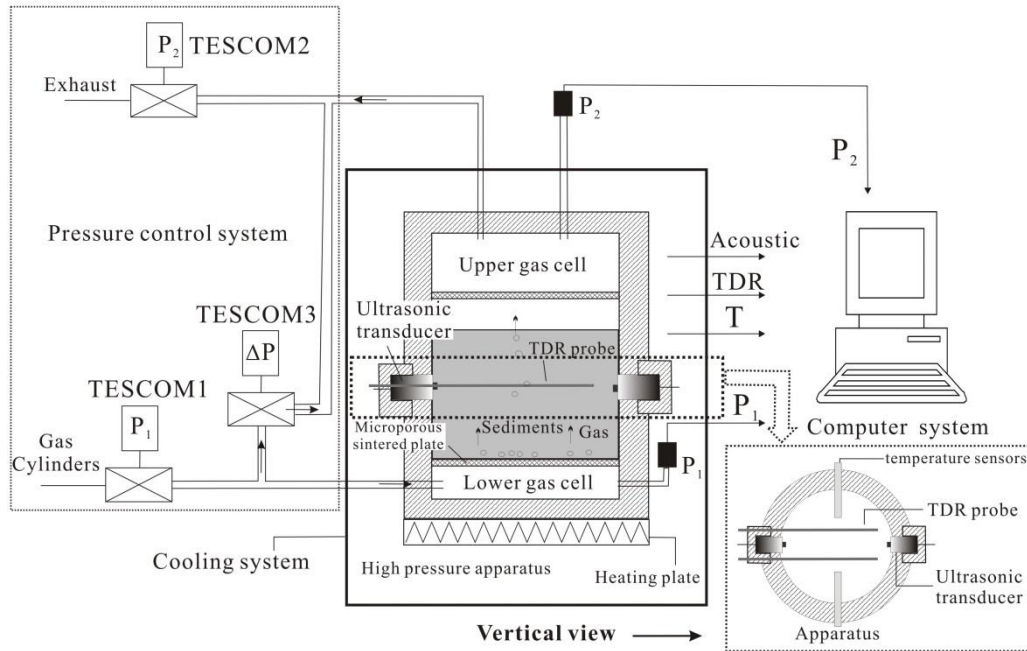

Figure 1. Gas hydrates geophysical simulation equipment for a vertical gas migration system (TESCOM means Tescom electrically controlled pneumatic valve)

The computer control system consists of a computer, a Programmable Logic Controller (PLC), Pt100 temperature sensors, pressure sensors, TDR probe and

ultrasonic transducers. The TDR test system consists of a signal generator, two needle probes, test tube and a computer. The type of TDR signal generator is TDR100 which is produced by American Campbell Scientific company. TDR is used to measure water content, the probe length is 0.16 m with precision of $\pm(2\%\sim2.5\%)$ (Wright *et al*., 2002). P wave and S wave signals were collected by transmission using two transducers placed at both sides of the sediment samples.

The unconsolidated sediment sample used in this experiment is sieved natural sand with grain sizes of 0.425~0.85 mm, its porosity is 39%. During methane hydrate formation, sodium dodecyl sulfate (SDS) solution (300 ppm) is used to enhance the formation speed.

3. Measuring Methods

3.1. Hydrate Saturation Measurements

Hydrate saturation was measured by TDR. The propagation velocity of the electromagnetic wave in the samples was different due to the different dielectric constant (Dalton *et al.*,1984), from which we can obtain a TDR waveform and then calculate the water content / hydrate saturation (see equations 3 and 4 below) (Wright *et al.*, 2002). A TDR100 unit and a pair of TDR probes were used in the experiment. The TDR technology was initially used by Wright *et al.* (2002) to determine hydrate saturation, and was developed and frequently used in our laboratory since 2004 (e.g. Hu *et al.*, 2010a, 2012, 2014a). Their result suggested that the measurement accuracy of water content is $\pm2\sim2.5\%$. And the temperature (20~0.5℃) and pressure (1~7MPa) have small influences on water content measurements according to our tests (Ye *et al*., 2008). The error of water content caused by temperature is $\pm1.6\%$ (water content, $\pm0.73\%$), and the error of water content caused by pressure is $\pm0.5\%$ (water content, $\pm0.23\%$). Based on the TDR data obtained in the experiments, the water content (θ_V) of the sample was calculated by Wright's empirical equation (Wright *et al*., 2002). Subsequently, hydrate saturation was calculated by the equation $S_h=(\varphi-\theta_V)/\varphi\times100\%$, where φ is the porosity of the sample.

3.2. Wave Velocities Measurements

Ultrasonic methods were used to measure the wave velocities of hydrate-bearing

sediment. P-wave and S-wave velocities were measured by ultrasonic transmission methods, two transducers (112 KHz frequency) were placed on each side of the sediment sample. A CompuScope card from Gage Corporation in Canada digitized the signals. The CompuScope 14100 is 14 bit 50 MS/s dual channel waveform digitizer card and data transfer rates from the CompuScope memory to PC memory is 80 MB/s, so the CompuScope card may cause few errors in velocity estimation. However, the error of velocity estimation is mainly from picking the traveltimes of the compressional and shear wave. The velocities are calculated by V_p=L/(t$_1$-t$_0$) and V_s=L/(t$_2$-t$_0$), where L is the sample length and t$_0$ is the inherent traveltime of the transducers, t$_1$ and t$_2$ are the traveltimes of the compressional and shear wave, respectively. Four different lengths of standardized polyoxymethylene (POM) rods were used to calibrate the t$_0$ of the transducers. The calibrate of the ultrasonic transducers is introduced in supplementary materials (S2).

The measurements of V_p, V_s and water saturation (hydrate saturation) are independent, and the probes arranged inside the reaction vessel do not interfere with each other. The traveltimes of the P- and S- waves are picked based on the software, and then the velocities of the P- and S- waves are calculated as following:

$$V_p = \frac{L}{t_p - t_{0p}} \tag{1}$$

$$V_s = \frac{L}{t_s - t_{0s}} \tag{2}$$

Where L is the distance between the ultrasonic probes, t_{0p} and t_{0s} are the inherent traveltime of the transducers, t_p and t_s are the traveltimes of the P- and S- waves, respectively.

For hydrate-bearing sediments, the empirical formula of Wright *et al.* (2002) is mainly used:

$$ɜ_v = -11.9677 + 4.506072566K - 0.14615K^2 + 0.0021399K^3 \tag{3}$$

Here, θ_V represent the water content, K represent the dielectric constant.

And the hydrate saturation can be calculated by the porosity (φ) and water

content (θ_V) of the samples:

$$S_h = (\varphi - \theta)/\varphi \times 100\%$$ (4)

4. Novel Aspects of the Vertical Gas Migration System

As mentioned above, it is difficult to form hydrate in gas migration system. Three main problems need to be solved to achieve the vertical gas migration system.

4.1. The Pressure Control of Vertical Gas Migration

The key point in the pressure control system is the appropriate pressure range between the inlet P_1 and the outlet P_2. The pressure is considered to be appropriate if ΔP ($\Delta P = P_1 - P_2$) can make gas migrate through the sediment slowly from bottom to top and not take away the water from the sediment. The appropriate pressure ΔP is set up to 0.3 MPa according to several tests.
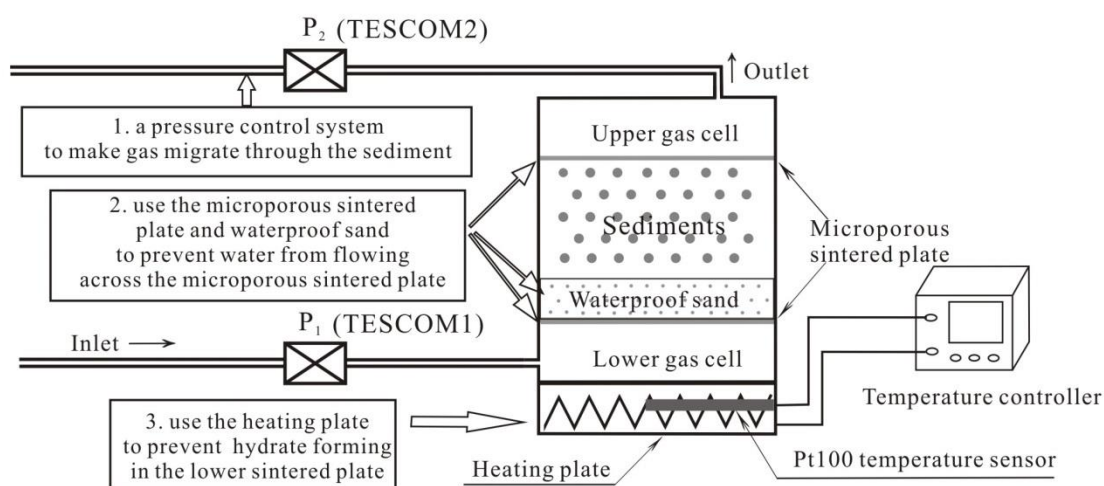

Figure 2. Vertical gas migration system in apparatus

4.2. The Application of Microporous Sintered Plate and Waterproof Sand

Water in the sediments should not be taken away by gas flow or leak out. The microporous sintered plate (Figure 2) can let gas go through and prevent water from moving in the sediments. In order to prevent water from flowing across the microporous sintered plate which is between the sediments and the lower gas cell, waterproof sands are made and put under the sediments. Waterproof sands are made from common sands whose surface is covered with waterproof material.

Several tests were taken to examine the waterproof sand. As shown in table 1, tests use four 25ml cylinders (diameter 1.5cm) which numbered 1, 2, 3, 4 respectively.

The four cylinders are filled with different grain sizes of sands. The four cylinders are placed horizontally on the desktop, adding water to the same height after the water level dropped down according to the permeation, and then left them for 24 hours. As waterproof sands are not placed in No.1 and No.2, sands in the two cylinders have been completely wet. Conversely, bottom sands in No.3 and No.4 are still dry as waterproof sands in the upper layers (Figure 3). Thus waterproof sand can prevent water well, it can let the gas pass and leave the water in the sediment .

Table 1. Distribution of sands and water in the cylinder

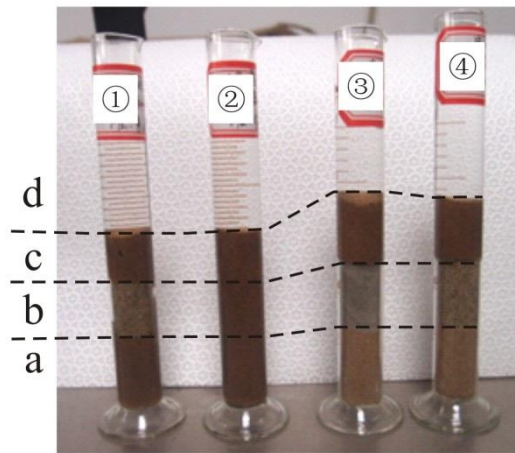| number	lower layer(a)	middle layer(b)	upper layer(c)	top layer(d)
1	0.125-0.18mm common sand	0.15-0.35mm common sand	0.125-0.18mm common sand	water
2	0.125-0.18mm common sand	0.125-0.18mm common sand	0.125-0.18mm common sand	water
3	0.125-0.18mm common sand	0.063-0.09mm waterproof sand	0.125-0.18mm common sand	water
4	0.125-0.18mm common sand	0.15-0.35mm waterproof sand	0.125-0.18mm common sand	water

Figure 3. Contrast the waterproof effect between waterproof sand and common sand

4.3. The Application of Heating Plate

As the gas migration channel could be blocked by forming hydrate in the lower sintered plate, we design a heating plate (Figure 2) under the lower gas cell to solve the problem. The heating plate will heat the apparatus wall around the lower gas cell, when gases move across the sintered plate into sediments, the microporous sintered plate will have a slightly higher temperature than the hydrate formation temperature,

so hydrate can hardly form in the bottom and the gas channel could not be blocked.

5. Hydrate Formation Process and Results

The process of elastic wave studies on gas hydrate in vertical gas migration system is as follows:

(1) Putting the inner barrel, ultrasonic probe, TDR probes, Pt100 probes and sintered plate into the apparatus.

(2) Putting a layer of waterproof sands at the bottom of the apparatus with a thickness of about 3 cm. And then adding the common sand upon the waterproof sands with 85% water saturation (300 ppm SDS solution + dried common sands with grain size of 0.425 - 0.85 mm).

(3) Compacting the common sands in the apparatus and covering the sediments space with microporous sintered plate.

(4) Increasing the system pressure with a desired pressure at 6 MPa. The upper and lower gas cell pressure become stable after the boost process, then setting the pressure difference with 0.3 Mpa, the inlet valve is kept open during the hydrate formation process.

(5) Putting the apparatus in the air bath cooling system, turn on the incubator and set the temperature at 2 ℃. Open the heating plate under the lower gas cell.

(6) Turn off cooling system when the saturation of hydrate is no longer rising, and then close the heating plate and the inlet valve of the apparatus, gas hydrate begin to dissociate as the temperature increase.

Experiments on gas hydrate formation in vertical gas migration system have been conducted for six runs, the first two runs of the experiments did not use the heating plate while the later four runs used. Taking the second and the fourth run as examples to describe hydrate formation and dissociation process.
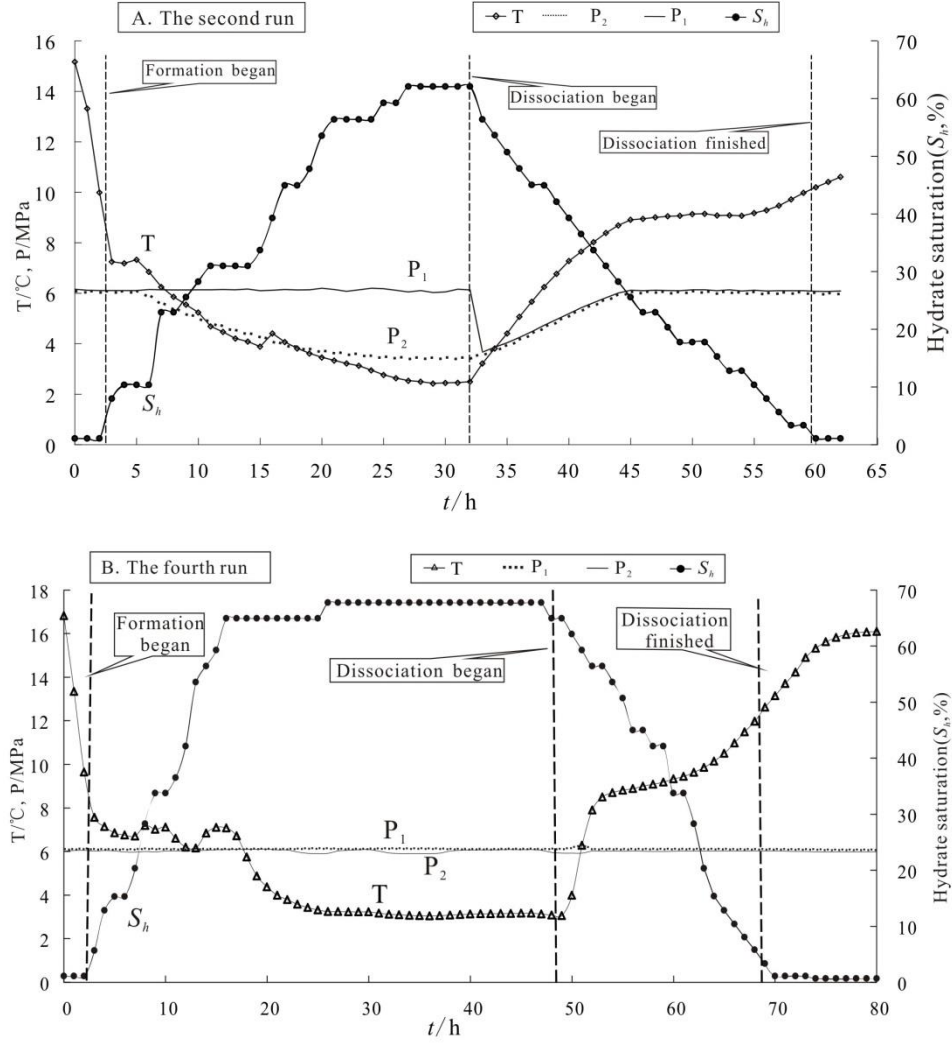
Figure 4. The change of temperature, pressure, saturation with hydrate formation and

dissociation (the second run, the fourth run)

The initial pressure in the apparatus is 6 MPa as shown in figure 4. At 0 ~ 3 h, the temperature continued to decrease from 15.17 ℃ to 7 ℃ with no hydrate formed in the sediments. The pressures in the upper and lower gas cell (P_2, P_1) are stable at 6 MPa. And then the hydrate began to form as the temperature decreasing. In the second run (not use heating plate) the lower gas cell pressure P_1 was still able to remain at 6.1 MPa due to the continued gas supply, while the upper gas cell pressure P_1 began to decrease. The decreasing of the pressure P_2 maybe caused by the following reasons: the CH_4 gas was consumed as hydrate began to form; the temperature was decreasing; the gas migration channel was blocked as the hydrate formed, so the upper gas cell could not obtain enough gas. However, in the fourth run experiment (use heating plate)

the lower gas cell pressure P_2 and the upper gas cell pressure P_1 did not change much.

The temperature, the upper and lower pressure and the hydrate saturation were maintained for a period of time (the second run at 26 - 32 h, the fourth run at 26 - 48 h) and found no further changes, which indicates that the hydrate formation process had finished. After the maximum hydrate saturation, although we kept the condition for hours, but the hydrate formation is so slowly that we cannot detect change in laboratory, perhaps hydrate formation can go on if time is enough (such as in the geological time scale). After the hydrate formation ended, turn off the incubator and the heating plate, the temperature will increase to the room temperature and the hydrate began to dissociate. In the second run the unicom control valve was opened by a manual operation, the upper pressure P_2 and lower pressure P_1 soon maintained at 3.6 MPa, at this time the hydrate dissociated quickly due to the decreasing of the pressure and the increasing of the temperature. The pressure increased to 6 MPa as the hydrate dissociated, excess gases will exhaust via the back pressure valve and at last the pressure P_1 and P_2 maintained at 6 MPa. As the temperature continued to increase, the hydrate dissociated completely in the end of the experiment.

Table 2. Experimental data of the fourth run

Time/h	T/℃	Upper gas cell pressure P_2/Mpa	Lower gas cell pressure P_1/Mpa	Hydrate saturation (S_h)/%	Vs(m/s)	Vp(m/s)
0	16.82	6.02	6.11	0.00	712.37	1721.82
1	13.34	6.05	6.11	0.00	714.55	1735.58
2	9.65	6.06	6.13	0.00	812.48	1807.64
3	7.57	6.02	6.11	5.64	819.98	1852.87
4	7.14	6.05	6.11	12.79	823.60	1861.68
5	6.85	6.03	6.10	15.26	822.23	1938.95
6	6.75	5.98	6.10	15.26	826.11	1946.88
7	6.71	5.97	6.10	20.34	852.98	1948.45
8	7.20	6.01	6.13	28.26	859.62	2003.63
9	7.02	5.99	6.12	33.72	863.33	2018.66
10	7.11	6.02	6.12	33.72	861.47	2049.68
11	6.60	6.03	6.11	36.49	862.26	2053.19
12	6.20	6.04	6.12	42.12	862.02	2048.32
13	6.16	6.05	6.13	53.53	935.95	2226.43
14	6.84	6.06	6.12	56.40	962.93	2225.23
15	7.11	6.08	6.12	59.25	1026.86	2243.44

16	7.08	6.09	6.12	64.91	1026.86	2246.30
17	6.72	6.10	6.12	64.91	1026.86	2246.30
18	5.75	6.10	6.12	64.91	1026.86	2365.37
19	4.88	6.10	6.13	64.91	1031.38	2365.37
20	4.38	6.11	6.12	64.91	1163.27	2365.37
21	3.99	6.08	6.12	64.91	1159.25	2417.28
22	3.79	6.08	6.12	64.91	1165.39	2417.28
23	3.58	5.98	6.13	64.91	1183.98	2470.65
24	3.43	5.92	6.14	64.91	1159.25	2470.65
25	3.31	5.91	6.14	64.91	1171.39	2498.67
26	3.25	5.92	6.14	67.71	1165.39	2498.67
27	3.25	6.03	6.13	67.71	1161.74	2498.67
28	3.24	6.06	6.12	67.71	1145.25	2498.67
29	3.23	6.08	6.12	67.71	1183.98	2555.74
30	3.23	6.09	6.13	67.71	1188.97	2523.72
35	3.06	5.91	6.14	67.71	1182.79	2582.89
40	3.13	6.07	6.11	67.71	1184.18	2549.27
45	3.17	6.08	6.12	67.71	1158.87	2519.21
47	3.14	6.06	6.11	67.71	1158.87	2519.21
49	3.06	5.93	6.12	64.91	1164.81	2496.90
50	3.99	5.93	6.18	62.09	1160.02	2435.65
51	6.29	5.93	6.29	59.25	1136.27	2378.14
52	7.91	6.02	6.12	56.40	1087.38	2240.58
53	8.50	6.01	6.12	56.40	959.90	2204.16
54	8.71	6.02	6.12	53.53	958.08	2195.92
55	8.82	6.01	6.11	50.67	876.59	2127.66
56	8.88	6.02	6.12	44.96	863.92	1953.18
57	9.00	6.01	6.12	44.96	787.75	1924.39
58	9.09	6.01	6.12	42.12	782.85	1916.02
59	9.18	6.01	6.12	42.12	762.04	1910.83
60	9.33	6.01	6.12	33.72	762.78	1906.18
61	9.44	6.02	6.12	33.72	765.18	1907.73
62	9.64	6.02	6.12	28.26	762.86	1894.91
63	9.86	6.02	6.12	20.34	759.08	1881.76
64	10.15	6.02	6.12	15.26	758.51	1856.97
65	10.51	6.03	6.12	12.79	740.82	1841.45
66	10.98	6.02	6.11	10.37	740.82	1841.45
67	11.49	6.02	6.11	7.98	724.01	1796.87
68	11.98	6.03	6.11	5.64	724.97	1796.87
69	12.62	6.03	6.11	3.34	724.97	1796.87
70	13.15	6.03	6.11	1.08	726.39	1768.47
75	15.62	5.99	6.08	0.64	724.97	1782.78
80	16.10	5.99	6.08	0.64	688.98	1715.95

As shown in figure 5 (the original data of the fourth run are shown in Table 2),

the acquired temperature and pressure data, the wave velocities and the hydrate saturation data can all reflect the process of gas hydrate formation and subsequent dissociation. At the beginning of hydrate formation the temperature had an abnormal rise due to the exothermic process, at the same time the corresponding hydrate saturation increased rapidly, reflecting the hydrate formed severely. The wave velocities increased as the hydrate increased the bulk modulus and shear modulus of sediments and decreased the density.

Figure 5. The change of temperature, pressure, saturation and acoustic velocity (the fourth run)

6. Discussion

6.1. Velocity Characteristics in a Vertical Gas Migration System

The experimental system meets the gas hydrate formation condition as it has a suitable temperature and pressure, sufficient pore space and water, and it also has a vertical gas migration system to simulate the real hydrate accumulation environment.

The results of the six run experiments showed that the changes of velocities agree well with the change of hydrate saturation, indicating that the experiment has good reproducibility. Here, we take the fourth experimental run as an example to describe the behavior of ultrasonic velocities during hydrate formation and dissociation (Figure. 5). The results showed that at the beginning of the hydrate

14

formation, the velocities of hydrate-bearing sediments had a rapid increase as the hydrate saturation increased, then the velocities increased slowly, and finally the velocities increased rapidly again when the hydrate saturation reached 60%. At the initial stage of dissociation, the velocities decreased quickly, then the velocities decreased slowly with the decreased hydrate saturation. At the beginning of the experiiment the compressional wave velocity and shear wave velocity are 1702m/s and 712m/s, respectively. The saturation of the hydrate can reach 67% when the hydrate formed completely, and the compressional wave velocity and shear wave velocity increased to 2580m/s and 1184m/s.

The relationship between the ultrasonic velocities of hydrate-bearing sediments and hydrate saturation has been established based on the experimental data, as shown in figure 6 and figure 7. When hydrate saturation is lower than 50%, V_p and V_s in the hydrate formation process is bigger than that in the hydrate dissociation process at the same hydrate saturation. This result matches well the observed relationship between the ultrasonic velocities and hydrate saturation in sediments inside a closed system by Hu *et al.* (2012). The elastic velocities of the sediment frame are easily influenced by the morphology of hydrate, hydrates cement the sediment grains during hydrate formation and increase the contact area between the grains, so the velocities of the sediment increase sharply (Priest *et al.*, 2005), and then hydrates continue to cement the sediment grains, or form in the pore fluid. We may infer that if hydrates dissociate at grain contacts first, the process may destroy the cementation between the grains, so the dissociation process would lead to a lower velocity compared to the hydrate formation process. The results show that velocities increase at a constant rate with hydrate saturation when the heating plate is not used (the second run). However, when we use the heating plate (the fourth run), the velocities have a very small initial increase with hydrate saturation between 0 - 20%, while the velocities increase slower for hydrate saturations between 20% - 60%, and when the saturation is higher than 60%, the velocities increase faster again. Overall, the increasing velocities show a fast-slow-fast process with increasing hydrate saturation.
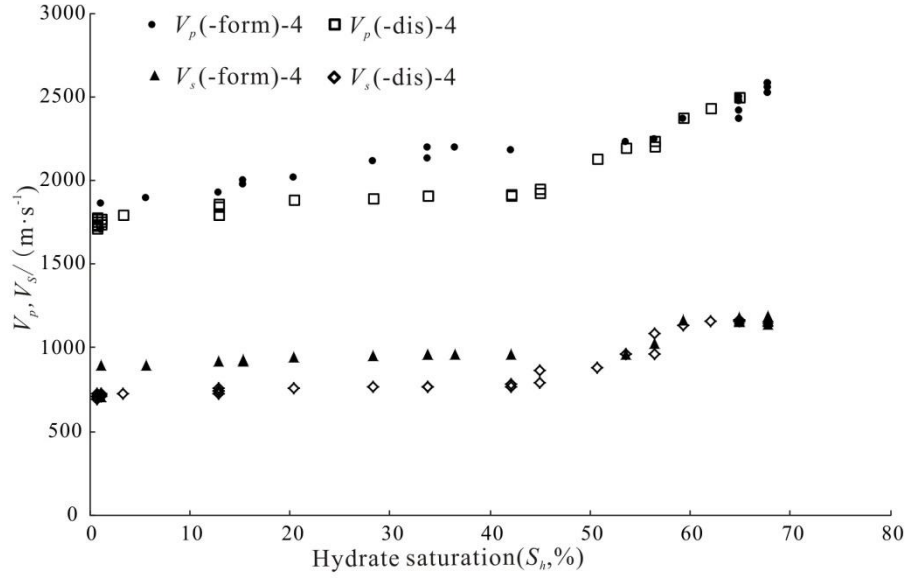
Figure 6. Variation in P- and S-wave velocities with hydrate saturation during hydrate formation and dissociation (fourth run)

6.2. Comparison of Velocity Characteristics between the Vertical Gas Migration and the Closed Systems

The velocities acquired in this study are different from the results of Hu *et al.* (2012) which were obtained in sediments (grain size 0.09 - 0.125mm) under closed conditions and other data in the reference (Figure 7). The results show that the obtained P-wave velocity at a saturation lower than 20% consistent with the result given by Ren *et al.* (2010), indicating that the distribution modes of hydrate may be cementing modes in both of the two experiments. The obtained P- and S- wave velocities at the same saturation are lower than those measured by Priest *et al.* (2005), the synthesized hydrate specimens are harder , so they have higher P- and S- wave velocities. Here, the velocities of the hydrate-bearing sediments increase at a constant speed, similar to the first two runs in this vertical migration system study (Figure 7, second run). As noted above, in the latter four runs the velocities increase faster in the initial stage, even though they increase more slowly than Hu *et al.* (2012) data, then the velocities plateau with hydrate formation, when the hydrate saturation reached to 60%, the velocities increase faster again. On the one hand, the change of the velocity may be influenced by the morphology of the hydrate during hydrate formation. In the coarser sand used in this study, hydrates cement firstly the sand grains and hence have

16

a greater impact on velocity, and then hydrate forms in the pore fluid with a less impact on velocity. In the finer sand used in the study of Hu *et al.* (2012), the hydrate may cement grains and easily bridge across the pore space, and both of these modes have a greater impact on velocity. On the other hand, as we know, in the system of gas migration into gas hydrate-bearing sediments in field, the hydrate stability zone has high velocities, and the low-velocity zone is free gas-charged (Bunz and Mienert, 2004; Crutchley *et al.*, 2015). And in the hydrocarbon leakage system, the low-velocity gas-charged zones always represent the leakage process (Løseth *et al.*, 2009). In our study, as the gas continuously migrate into the sediment, the presence of the flowing gas in sediments may decrease velocities, so the P-wave velocities increase slower in the last four runs. That is, the last four runs, the presence of free gas affects P-wave velocity until a lot of hydrates are formed when velocities start to rise to the values observed by Hu *et al.* (2012) (although the current data only extend to S_h = 67% as opposed to 100% for Hu *et al.*).

The results show that both in a closed system (Figure 7; Hu *et al.*, 2012) and in a vertical gas migration system (this study), elastic wave velocities in hydrate-bearing sediments increase with hydrate saturation. However, the velocity increases are affected by different processes in the two systems. In the closed system, velocities show a stable increasing trend with more subtle rate stage changes. In the vertical gas migration system, the P-wave velocities increase slower in the later four runs (Figure 7). As hydrates grow in the sediments, hydrates in "floating" mode will eventually start to contact, or bridge between the grains; hence, when hydrate saturation reaches to a certain value, the velocities start to increase faster again when hydrate contributes to the elastic stiffness of the sediments frame. This is the case for the latter four runs when hydrates saturation reached to 60%. So during the process of hydrate formation, P-wave vecolities in a vertical gas migration system are smaller than in the closed system, the increasing P-wave velocities show a fast-slow-fast process with hydrate saturation, while the increasing trend of S-wave velocities changes little. The hydrate formation characteristics are different between the vertical gas migration system and the closed system.
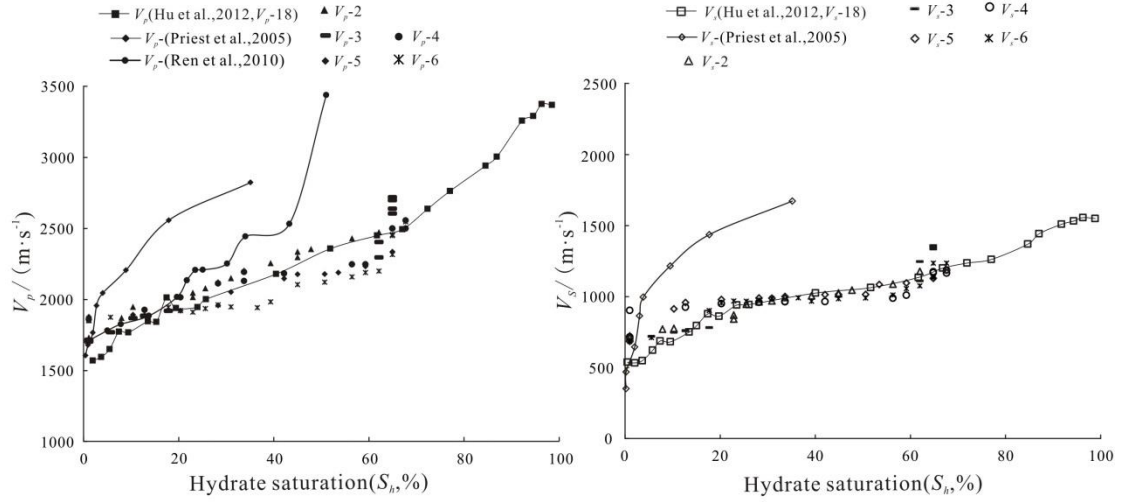
Figure 7. Contrast in the relationship between hydrate saturation and elastic wave velocities for a closed system (Hu *et al.*) and a vertical gas migration system (this study)

6.3. *The Morphology of Hydrate During the Hydrate Formation Process*

The above results show that the nature of the gas supply influences hydrate morphology to an extent that affects elastic wave velocities. The methane gas moves across the sediments continuously during the experiments in this study. According to the pressure ΔP and the parameters of the apparatus, we may calculate the methane gas flux generally. The range of ΔP is 0.01 - 0.26 MPa, and the methane gas flux across the sediment samples may between 0.12 - 3.05 mol/(m^2 · s).

In order to explain the observed velocity changes better, the effective medium theory (EMT) of Dvorkin *et al.* (1999) and Helgerud *et al.* (1999) was used to calculate velocities of gas hydrate-bearing sediments with different idealized hydrate morphologies (see Appendix). Here, hydrate morphology is represented by three kinds of EMT model: pore-filling hydrate; grain contacting hydrate; and grain cementing hydrate. In Model A, hydrates are considered to be part of the pore fluids; in model B, hydrates are considered to be part of the sediment frame; in model C, the porosity is decreased as in model B, and the change of the bulk modulus and shear modulus should be amended based on cementation theory by Dvorkin *et al.*(1993). We use these models to infer the distribution of hydrates in our experimental sediment samples. Figures 8 and 9 compare results between the models and the measurements.

At the beginning of the hydrate formation, the measured results (the latter four runs) have a similar trend with the velocities calculated from EMT-C (cementing hydrate), and the measured results do not match well with the EMT models until the hydrate saturation up to 20%. And when the hydrate saturation is between 20% to 60%, the measured results (the latter four runs) are similar with the calculated results of the EMT-A. As we known, P-wave velocity is greatly affected by the free gas, but the presence of free gas did not change the S-wave velocity (Riedel *et al.*, 2014). The decrease in V_p/V_s ratio is more obvious than any change in either P- or S-wave velocity alone. V_p/V_s exhibit tends to be smaller with hydrate saturation. Since the compressional wave velocity and shear wave velocity increase with hydrate saturation, so the V_p/V_s ratio show that the increasing rate of the V_s is larger than V_p. In the initial and last stage of hydrate formation, V_p/V_s is similar with the calculated results of the EMT-C, V_p/V_s range is between the EMT-C and the EMT-A during hydrate formation process (Figure 9), while the measured data have the similar trend with the calculated results.
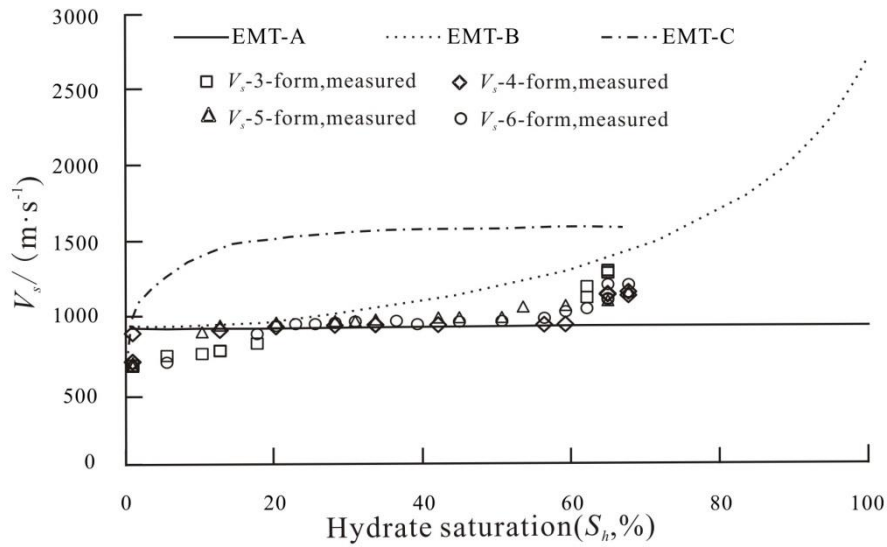

Figure 8. Measured V_s and the calculated V_s from the effective medium theory (EMT-A = pore-filling hydrate; EMT-B = grain contacting hydrate; EMT-C = cementing hydrate)
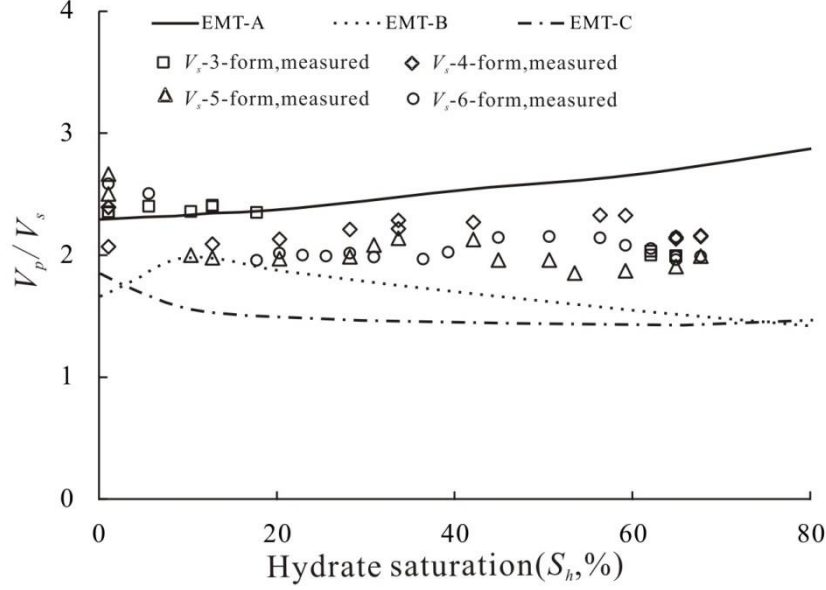
Figure 9. Measured V_p/V_s and the calculated V_p/V_s from the effective medium theory (EMT-A = pore-filling hydrate; EMT-B = grain contacting hydrate; EMT-C = cementing hydrate)

In summary, our previous laboratory studies have observed effects on elastic wave velocities due to changing methane hydrate morphology during hydrate formation. We have observed the in-situ pore scale distribution of gas hydrate directly based on the x-ray computerized tomography (X-CT). The results show that hydrates mainly cement sediment grains in the initial stage of formation, and contact (bridge) grains or float in the pore fluid in the intermediate stage, and finally hydrates cement grains again in the last stage (Hu *et al.*, 2014b). Hydrates have various growth patterns with different hydrate saturation, the sediment stiffness can be increased by a small amount of hydrate (Dai *et al.*, 2012). Priest *et al.* (2009) reported that hydrates preferentially formed at grain contacts when hydrate was formed under excess gas conditions. Sultaniya *et al.* (2015) also found that, using the excess gas method, hydrates initially formed at grain contacts and also dissociated at grain contacts first. According to our new experimental data, comparison to effective medium models, and with reference to previous research, we can draw conclusion about changing hydrate morphology during formation in our experiments (Figure 10).

At the beginning of the reaction, the hydrate saturation is small and the wave velocities increase fast, hydrates preferentially form at grain contacts by cementation

20

and on the surface of gas bubbles (Figure 10b), and the sediment grains will be bonded by the hydrate shell that is formed. Then the wave velocities increase slowly with hydrate satuation, and as shown in figure 8 and 9, the measured results are a little smaller than the floating model, maybe this is affected by the existence of the gas flow. The hydrate formation process is difficult than that in the closed system as gas bubbles migrate through the system. The hydrates mainly formed inside the pore fluid (floating hydrate) in this stage (Figure 10c). Then as hydrate saturation increases, the floating hydrate comes into contact with the sediment grains and hence stiffens the sediment frame with the increasing hydrate saturation (Figure 10d), so the wave velocities increase faster. This is not a linear relationship between wave velocity and hydrate saturation during formation. As gas migrates continuously in the system, there will be always a gas flow channel in the sample though in the end of hydrate formation (Figure 10d). During hydrate dissociation, hydrates first dissociate at the grain contacts, because sand has a higher thermal conductivity than methane or hydrate (Cortes *et al.*, 2009), and this will destroy the integrity of the hydrate cemented frame. Therefore, wave velocities decrease rapidly at the beginning of dissociation, and then velocities reduce more slowly as hydrates continue to dissociate.
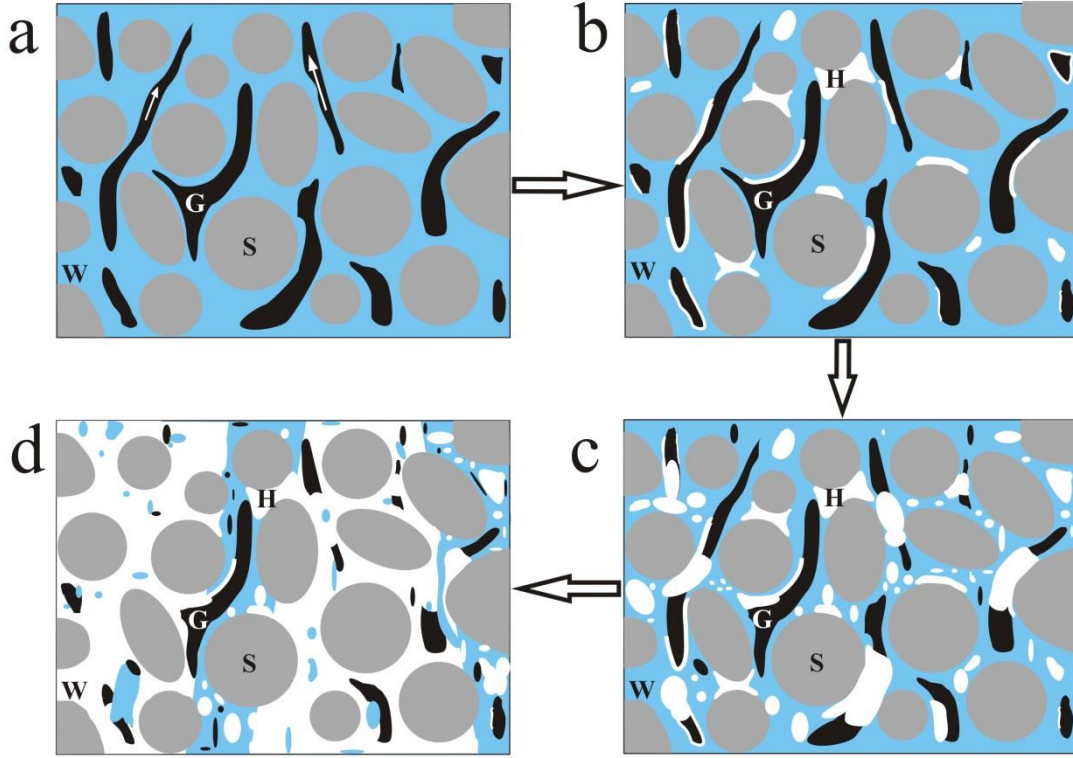
Figure 10. Conceptual model for hydrate growth in this experiment. (a) Before hydrate formation, (b) Hydrate nucleated first on the surface of gas bubble and at grain contacts, (c) Further hydrate formation grew across the entire sample (mainly in the pore fluid), (d) The end of hydrate formation (with gas flow channel in the sample). S is solid grain. W is water phase. H is hydrate phase. G is gas phase.

7. Conclusions

In this study we implemented novel methods to simulate a hydrate formation process under vertical gas migration. Several new aspects were needed to achieve the desired results: the introduction of a microporous sintered plate, waterproof sand, a heating plate, and a special pressure control system. Experiments were carried on to simulate hydrate formation under vertical gas migrations with real-time monitoring of temperature, pressure, P- and S-wave velocity and hydrate saturation (by TDR). We compared the velocity results to similar velocity data previously acquired in a closed system.

The results showed that V_p and V_s are higher during hydrate formation than during hydrate dissociation for the same hydrate saturation. During hydrate formation,

P-wave velocities in a vertical gas migration system are lower than those in a closed system. While velocities increase at a relatively constant rate with hydrate saturation in the closed system, P-wave velocities show a fast-slow-fast response to hydrate saturation in the vertical gas migration system. In this study, P-wave velocities increase faster with hydrate saturation between 0 - 20%, they increase more slowly between 20 - 60% hydrate saturation, and then increase faster again above hydrate saturations of 60%. S-wave velocities have the similar increasing tend with the closed system.

By comparison of our velocity observations to effective medium models for different idealized hydrate morphologies, we infer that hydrates preferentially form at grain contacts and on the surface of gas bubbles at the beginning of hydrate formation, then hydrates form in the pore fluid (floating hydrate), and lastly hydrates grown into contact with the sediment grains again as they fill up the pore spaces. During hydrate dissociation, hydrates firstly dissociate at grain contacts, thus weakening the frame elastic moduli and rapidly lowering velocities.

Appendix A

Effective Medium Theory

Effective medium theory is propose by Helgerud (1999) and Dvorkin (1999), mainly for unconsolidated sediments with high porosity. Ecker (2001) proposed three kinds of microscopic models for hydrate-bearing sediments, and three formulas are given according to the three models in the effective medium theory. In Model A, hydrates are considered to be part of the pore fluids; in model B, hydrates are considered to be part of the sediment frame, and two effects are produced, it not only decreases the porosity, but also change the bulk modulus and shear modulus of the matrix; in model C, the porosity is decreased as in model B, and the change of the bulk modulus and shear modulus should be to be amended based on cementation theory by Dvorkin *et al.*(1993). The calculation of the three models are as follows:

Model A of the effective medium theory

The formula of P wave velocity V_p and the bulk density ρ_b are given as follows:

$$V_p = \sqrt{\frac{K_{sat} + \frac{4}{3} G_{sat}}{\rho_b}} \qquad (A\text{-}1)$$

$$\rho_b = (1 - \varphi)\rho_s + \varphi\rho_f \qquad (A\text{-}2)$$

Where, K_{sat} and G_{sat} are the bulk modulus and shear modulus of the effective medium, respectively; ρ_s and ρ_f are the bulk density in rock solid and fluid phases. Both of the densities can be calculated by arithmetic mean of density based on the volume percentage of the components, φ_c is the critical porosity, and generally take 0.36 ~ 0.40 (Nur *et al.*, 1995). When sediments are filling of fluids with the bulk modulus K_f, according to Gassmann equation, the bulk modulus and shear modulus of the sediments can be given by the following formulas:

$$K_{sat} = K_{ma} \frac{\varphi K_{dry} - (1 + \varphi)K_f K_{dry}/K_{ma} + K_f}{(1 - \varphi)K_f + \varphi K_{ma} - K_f K_{dry}/K_{ma}} \qquad (A$$

$$-3)$$

$$G_{sat} = G_{dry} \qquad (A\text{-}4)$$

where K_{ma} and K_f are bulk modulus of the matrix and the pore fluid, respectively. K_{dry} and G_{dry} are bulk modulus and shear modulus of the dry rock. In mode A, hydrates formed in the pores, thus K_f is given as follows:

$$K_f = \left[\frac{1 - S_h}{K_w} + \frac{S_h}{K_h} \right]^{-1} \qquad (A\text{-}5)$$

Where S_h and K_h are hydrate saturation in pore space and the bulk modulus of hydrate, K_w is the bulk modulus of water. The formulas of K_{dry} and G_{dry} are given as follows:

$$K_{dry} = \begin{cases} \left[\dfrac{\varphi/\varphi_c}{K_{HM} + \frac{4}{3} G_{HM}} + \dfrac{1 - \varphi/\varphi_c}{K_{ma} + \frac{4}{3} G_{HM}} \right]^{-1} - \dfrac{4}{3} G_{HM}, \varphi < \varphi_c \\[4mm] \left[\dfrac{(1 - \varphi)/(1 - \varphi_c)}{K_{HM} + \frac{4}{3} G_{HM}} + \dfrac{(\varphi - \varphi_c)/(1 - \varphi_c)}{\frac{4}{3} G_{HM}} \right]^{-1} - \dfrac{4}{3} G_{HM}, \varphi \geq \varphi_c \end{cases} \qquad (A-$$

$$6)$$

$$
G_{dry} = \begin{cases} \left[\dfrac{\varphi/\varphi_c}{G_{HM} + Z} + \dfrac{1 - \varphi/\varphi_c}{G_{ma} + Z} \right]^{-1} - Z, \quad \varphi < \varphi_c \\[4mm] \left[\dfrac{(1 - \varphi)/(1 - \varphi_c)}{G_{HM} + Z} + \dfrac{(\varphi - \varphi_c)/(1 - \varphi_c)}{Z} \right]^{-1} - Z, \quad \varphi \geq \varphi_c \end{cases}
\tag{A-7}
$$

$$
Z = \frac{G_{HM}}{6} \left(\frac{9K_{HM} + 8G_{HM}}{K_{HM} + 2G_{HM}} \right)
\tag{A-8}
$$

Where,

$$
K_{HM} = \left[\frac{n^2 (1 - \varphi_c)^2 G_{ma}^2}{18\pi^2 (1 - \upsilon)^2} P \right]^{\frac{1}{3}}, G_{HM} = \frac{5 - 4\upsilon}{5(2 - 4\upsilon)} \left[\frac{3n^2 (1 - \varphi_c)^2 G_{ma}^2}{2\pi^2 (1 - \upsilon)^2} P \right]^{\frac{1}{3}}
\tag{A-9}
$$

where P is effective pressure, K_{ma} and G_{ma} are bulk modulus and shear modulus of the matrix, υ is Poisson's ratio of the rock matrix, and $\upsilon = 0.5 \left(K_{ma} - \frac{2}{3} G_{ma} \right) \Big/ \left(K_{ma} + G_{ma}/3 \right)$; n is the average number of contact grains in bulk unit, generally take 8~9.5.

Model B of the effective medium theory

hydrate is considered to be part of the matrix in Model B, it not only decreases the porosity, but also change the bulk modulus and shear modulus of the matrix. Therefore, based on the model A, the sediment porosity need to be amended, $\varphi_r = \varphi(1 - S_h)$. At the same time, hydrate should be taken as a mineral component in the formula to calculate the K_{ma} and G_{ma}. In addition, water is the only pore fluid in the sediment. Since the hydrate decreases the porosity, we should pay attention to the porosity φ_r and φ_c when calculate K_{dry} and G_{dry}, select the appropriate formula in formula (A-6) and (A-7).

We can account for the distribution dependant effects of gas on the sediment's elastic properties by modifying the calculation of the sediment's saturated bulk modulus (K_{sat}). If we consider the effects of gas, the bulk modulus of pore fluid (K_f) is given as follows:

$$
K_f = \left[\frac{S_w}{K_w} + \frac{1 - S_w}{K_g} \right]^{-1}
\tag{A-10}
$$

Where K_w and K_g are the bulk modulus of water and gas, and S_w is the water saturation.

Model C of the effective medium theory

in model C, the porosity is decreased as in model B, and the change of the bulk modulus and shear modulus should be to be amended based on cementation theory by Dvorkin et al. (1993). Thus, the calculation of φ_r, K_{ma}, G_{ma}, K_f and ρ_f are as same as in model B, K_{dry} and G_{dry} are given as the following formula:

$$K_{dry} = \frac{1}{6} n(1 - \varphi)\left(K_h + \frac{4}{3}G_h\right)S_n \tag{A-11}$$

$$G_{dry} = \frac{5}{3} K_{dry} + \frac{3}{20} n(1 - \varphi)G_h S_\tau \tag{A-12}$$

where S_n and S_τ are parameters which have positive correlation with cemented pressure and the amount of hydrate, the formulas are as follows:

$$S_n = A_n(\Lambda_n)\alpha^2 + B_n(\Lambda_n)\alpha + C_n(\Lambda_n) \tag{A-13}$$

where,

$A_n(\Lambda_n) = -0.024153\Lambda_n^{-1.3646}$,

$B_n(\Lambda_n) = 0.20405\Lambda_n^{-0.89008}$,

$C_n(\Lambda_n) = 0.00024649\Lambda_n^{-1.9864}$,

$$S_\tau = A_\tau(\Lambda_\tau, \upsilon)\alpha^2 + B_\tau(\Lambda_\tau, \upsilon)\alpha + C_\tau(\Lambda_\tau, \upsilon) \tag{A-14}$$

$A_\tau(\Lambda_\tau, \upsilon) = -10^{-2}(2.26\upsilon^2 + 2.07\upsilon + 2.3)\Lambda_\tau^{0.079\upsilon^2 + 0.1754\upsilon - 1.342}$

$B_\tau(\Lambda_\tau, \upsilon) = (0.0573\upsilon^2 + 0.0937\upsilon + 0.202)\Lambda_\tau^{0.0274\upsilon^2 + 0.0529\upsilon - 0.8765}$

$C_\tau(\Lambda_\tau, \upsilon) = 10^{-4}(9.654\upsilon^2 + 4.945\upsilon + 3.1)\Lambda_\tau^{0.01867\upsilon^2 + 0.4011\upsilon - 1.8186}$

$\Lambda_n = \dfrac{2G_h}{\pi G}\dfrac{(1 - \upsilon)(1 - \upsilon_h)}{1 - 2\upsilon_h}; \Lambda_\tau = \dfrac{G_h}{\pi G}; \alpha = \left[\dfrac{2S_h}{3(1 -)}\right]^{0.5};$

Where, G_h and υ_h are shear modulus and Poisson's ratio of hydrate, α is the radius ratio of cemented particles and sedimentparticles after hydrate cemented sediments particles.

26

$$K_{ma} = \frac{1}{2}\left[\sum_{i=1}^{m} f_i K_i + \left(\sum_{i=1}^{m} f_i / K_i\right)^{-1}\right] \tag{A-15}$$

$$G_{ma} = \frac{1}{2}\left[\sum_{i=1}^{m} f_i G_i + \left(\sum_{i=1}^{m} f_i / G_i\right)^{-1}\right] \tag{A-16}$$

where m is the number of mineral constituents (hydrate acts as a mineral); f_i is the volumetric fraction of the i-th constituent in the matrix; and K_i and G_i are the bulk and shear moduli of the i-th constituent, respectively.

Appendix B

mineral composition and physical parameters of unconsolidated sediments

(Helgerud *et al.*, 1999; Dvorkin *et al.*, 1999)

Mineral	Content(%)	$\rho(g/cm^3)$	K(Gpa)	G(Gpa)
Magnetite	1.94	5.21	161	91.4
Amphibole	1.10	3.12	87	43
Epidote	0.55	3.4	106.2	61.2
Quartz	38.95	2.65	36.6	45
Feldspar	57.46	2.62	76	26
Water		1.032	2.5	0
Pure Hydrate		0.9	5.6	2.4
Gas		0.235	0.1	0

Notation

V_p	Compressional wave velocity, m s^{-1}.
V_s	Shear wave velocity, m s^{-1}.
S_h	Hydrate saturation in pore space; $0 \leq S_h \leq 1$, corresponding to 0% to 100% of pore space.
S_w	Water saturation
φ	Fractional porosity of the sample.
φ_c	The critical porosity.
φ_r	The amended porosity in Model B and C.
P	Pressure, MPa.
T	Temperature of inner of the sample, ℃.
K	Bulk modulus, GPa.

G	Shear modulus, GPa.
ρ_b	Bulk density, g cm^{-3}.
ρ_s	Bulk density in rock phase, g cm^{-3}.
ρ_f	Bulk density fluid phase, g cm^{-3}.
K_{ma}	Bulk modulus of matrix, GPa.
G_{ma}	Shear modulus of matrix, GPa.
K_{sat}	Bulk modulus of the effective medium, GPa.
G_{sat}	Shear modulus of the effective medium, GPa.
K_{dry}	Bulk modulus of the dry rock, GPa.
G_{dry}	Shear modulus of the dry rock, GPa.
K_f	Bulk modulus of pore fluid, GPa.
K_h	Bulk modulus of hydrate, GPa.
K_w	Bulk modulus of water, GPa.
K_g	Bulk modulus of gas, GPa.
G_h	Shear modulus of hydrate, GPa.
v	Poisson's ratio of the rock matrix.
m	The number of mineral constituents in matrix.
f_i	The volumetric fraction of the i-th constituent in matrix.
K_i, G_i	Bulk moduli and shear moduli of the i-th constituent, respectively.

References

Bunz S, and Mienert J 2004 Acoustic imaging of gas hydrate and free gas at the Storegga Slide *J. Geophys. Res-Sol. Ea.* 109 380-389

Carcione J M, and Gei D 2004 Gas-hydrate concentration estimated from P- and S-wave velocities at the Mallik 2L-38 research well, Mackenzie Delta, Canada *J.*

Appl. Geophys. 56 73-78

Chong Z R, Yang S H B, Babu P, Linga P and Li X S 2015 Review of natural gas hydrates as an energy resource: Prospects and challenges *Appl. Energy.* 162 1633–1652

Collett T S 2014 The gas hydrate petroleum system, Proceedings of the 8th International Conference on Gas Hydrates (ICGH8-2014), Beijing, China.

Cortes D D, Martin A I, Yun T S, Francisca F M, Santamarina J C and Ruppel C 2009 Thermal conductivity of hydrate-bearing sediments *J Geophys Res-Sol Ea.* 114 135-142

Crutchley G J, Fraser D R A, Pecher I A, Gorman A R, Maslen G and Henrys S A 2015 Gas migration into gas hydrate-bearing sediments on the southern Hikurangi margin of New Zealand *J Geophys Res-Sol Ea.* 120 725-743

Dai S, Santamarina J C, Waite W F and Kneafsey T J 2012 Hydrate morphology: Physical properties of sands with patchy hydrate saturation *J Geophys Res-Sol Ea.* 117(B11) 11205

Dalton F N, Herkelrath W N, Rawlins D S and Rhoades J D 1984 Time-domain reflectometry: simultaneous measurement of soil water content and electrical conductivity with a single probe *Science* 224 989-990

Dvorkin J, and Nur A 1993 Rock physics for characterization of gas hydrate. In: Howell DG (ed) The future of energy gases: United States Geological Survey Professional Paper 1570: 293–298

Dvorkin J, Prasad M, Sakai A and Lavoie D 1999 Elasticity of marine sediments: Rock physics modeling *Geophys. Res. Lett.* 26 1781-1784

Eaton M, Mahajan D, and Flood R 2007 A novel high-pressure apparatus to study hydrate-sediment interactions *J. Petrol. Sci. Eng.* 56 101-107

Ecker C 2001 Seismic characterization of methane hydrate structures.

Guan J A, Li D L, Zhou H X, Liang D Q and Wan L H 2012 A experimental system simulate formation and dissosiation of the leak gas hydrate (in Chinese with English abstract) *Nature gas industry* 32 1-4

Helgerud M B, Dvorkin J, Nur A, Sakai A and Collett T 1999 Elastic-wave velocity in

marine sediments with gas hydrates: Effective medium modeling *Geophys. Res. Lett.* 26 2021-2024

Holbrook W S, Gorman A R, Hornbach, M, Hackwith K L, Nealon J, Lizarralde D and Pecher I A 2002 Seismic detection of marine methane hydrate *Leading Edge* 21 686-689

Holbrook W S, Hoskins H, Wood W T, Stephen R A and Lizarralde D 1996 Methane hydrate and free gas on the blake ridge from vertical seismic profiling, *Science* 273 1840-1843

Hu G W 2010a Experimental Study on Acoustic Response of Gas Hydrates to Sediments from South China Sea (Ph. D. thesis). Faculty of Earth Sciences, China University of Geosciences, Wuhan, China.

Hu G W, Ye Y G, Zhang J, Liu C L, Diao S B and Wang J S 2010b Acoustic properties of gas hydrate-bearing consolidated sediments and experimental testing of elastic velocity models *J. Geophys. Res-Sol. Ea.* 115(B2) 481-492

Hu G W, Ye Y G, Zhang J, Diao S B, Liu C L, Wang H X and Wang J S 2008 Study on Gas Hydrate Formation-dissociation and Its Acoustic Responses in Unconsolidated Sands (in Chinese with English abstract) *Geoscience* 22 465-474

Hu G W, Ye Y G, Zhang J and Diao S B 2010c Micro-models of gas hydrate and their impact on the acoustic properties of the host sediments (in Chinese with English abstract) *Natural Gas Industry* 30 120-124

Hu G W, Ye Y G, Zhang J, Liu C L and Li Q 2014a Acoustic response of gas hydrate formation in sediments from South China Sea *Mar. Petrol. Geol.* 52 1-8

Hu G W, Li C F, Ye Y G, Liu C L, Zhang J and Diao S B 2014b Observation of gas hydrate distribution in sediment pore space *Chinese Journal of Geophysics-Chinese Edition* 57 1675-1682

Hu G W, Ye Y G, Zhang J, Diao S B and Liu C L 2012 Acoustic properties of hydrate-bearing unconsolidated sediments based on bender element technique *Chinese Journal of Geophysics-Chinese Edition* 55 3762-3773

Kwon T H and Cho G C 2009 Evolution of Compressional Wave Velocity during CO2 Hydrate Formation in Sediments *Energ. Fuel.* 23 5731-5736

Liu B, Pan H, Wang X H, Li F G, Sun C Y and Chen G J 2013 Evaluation of Different CH4-CO2 Replacement Processes in Hydrate-Bearing Sediments by Measuring P-Wave Velocity *Energies* 6 6242-6254

Løseth H, Gading M and Wensaas L 2009 Hydrocarbon leakage interpreted on seismic data *Mar. Petrol. Geol* 26 1304-1319

Michael D Max 2003 Natural Gas Hydrate in Oceanic and Permafrost Environments, New York:Springer

Milkov A V and Sassen R 2003 Preliminary assessment of resources and economic potential of individual gas hydrate accumulatiom in the Gulf of Mexico continental slope *Mar. Petrol. Geol* 20 111-128

Nur A M, Mavko G, Dvorkin J, and Gal D 1995 Critical porosity: a key to relating physical properties to porosity in rocks *Leading Edge* 14 878-881

Pecher I A, Henrys S A, Wood W T, Kukowski N, Crutchley G J, Fohrmann M, Kilner J, Senger K, Gorman A R, Coffin R B, et al. 2010 Focussed fluid flow on the Hikurangi Margin, New Zealand-Evidence from possible local upwarping of the base of gas hydrate stability *Mar. Geol.* 272 99-113

Priest J A, Best A I and Clayton C R I 2005 A laboratory investigation into the seismic velocities of methane gas hydrate-bearing sand *J. Geophys. Res-Sol. Ea.* 110 B04102

Priest J A, Rees E V L and Clayton C R I 2009 Influence of gas hydrate morphology on the seismic velocities of sands *J. Geophys. Res-Sol. Ea.* 114 B11205

Ren S R, Liu Y J, Liu Y X and Zhang W D 2010 Acoustic velocity and electrical resistance of hydrate bearing sediments *J. Petrol. Sci. Eng.* 70 52-56

Riedel M, Goldberg D, and Guerin G 2014 Compressional and shear-wave velocities from gas hydrate bearing sediments: examples from the india and cascadia margins as well as arctic permafrost regions *Mar. Petrol. Geol.* 58 292-320

Shipley T H, Houston M H, Buffier R T, Shaub F J, Mcmillen K, Ladd J W and Worzel J L 1979 Seismic evidence for widespread occurrence of Possible gas hydrate horizons on continental slopes and rises *AAPG Bull.* 63 2204-2213

Stoll R D 1974 Effeets of gas hydrate in sediments, In: KaPlanⅠ.Natural Gases in Marine Sediment. First Edition, New York, Springer, 235-248

Su K H, Sun C Y, Dandekar A, Liu B, Sun W Z, Cao M C, Li N, Zhong X Y, Guo X Q, Ma Q L, et al. 2012 Experimental investigation of hydrate accumulation distribution in gas seeping system using a large scale three-dimensional simulation device *Chem. Eng. Sci.* 82, 246-259

Sultaniya A K, Priest J A and Clayton C R I 2015 Measurements of the changing wave velocities of sand during the formation and dissociation of disseminated methane hydrate *J Geophys Res-Sol Ea* 120 778-789

Tueholke, B E, Bryan G M and Ewing J I 1977 Gas hydrate horizons deteeted in seismic-profile data from the western North Atlantic, *Am. Assoc. Petrol.Geol.Bull.* 61, 698-707

Waite W F, Santamarina J C, Cortes D D, Dugan B, Espinoza D N, Germaine J, Jang J, Jung J W, Kneafsey T J, Shin H, et al. 2009 Physical properties of hydrate-bearing sediments, *Rev. Geophys.* 47, RG4003

Wang Y B, Fan S S, Guan J A, Liang D Q and Feng Z P 2007 Experimental simulation of oceanic leakage hydrate formation (in Chinese with English abstract) *Natural Gas Geoscience* 18 596-600

Winters W J, Waite W F, Mason D H, Gilbert L Y and Pecher I A 2007 Methane gas hydrate effect on sediment acoustic and strength properties, *J. Petrol. Sci. Eng.* 56 127-135

Wright J F, Nixon F M, Dallimore S R and Matsubayashi O 2002 A method for direct measurement of gas hydrate amounts based on the bulk dielectric properties of laboratory test media, paper presented at 4th International Conference on Gas Hydrates, Tokyo Inst. of Technol., Yokohama, Japan.

Ye Y G, Zhang J, Hu G W, Diao S B and Liu C L 2008 Combined detection technique of ultrasonic and time domain reflectometry in gas hydrate (in Chinese with English abstract) *Marine Geology & Quaternary Geology* 28 101-107